Publication I

Piippo, A., Hinkkanen, M., and Luomi, J. (2004). “Sensorless control of PMSM drives using a combination of voltage model and HF signal injection.” In *Conference Record of the 39th IEEE-Industry Applications Society (IAS) Annual Meeting*, vol. 2, pp. 964–970, Seattle, WA.

© 2004 IEEE. Reprinted with permission.

This material is posted here with permission of the IEEE. Such permission of the IEEE does not in any way imply IEEE endorsement of any of the Helsinki University of Technology’s products or services. Internal or personal use of this material is permitted. However, permission to reprint/republish this material for advertising or promotional purposes or for creating new collective works for resale or redistribution must be obtained from the IEEE by writing to pubs-permissions@ieee.org.

By choosing to view this material, you agree to all provisions of the copyright laws protecting it.

Sensorless Control of PMSM Drives Using a Combination of Voltage Model and HF Signal Injection

Antti Piippo, Marko Hinkkanen, and Jorma Luomi
Power Electronics Laboratory
Helsinki University of Technology
P.O. Box 3000, FIN-02015 HUT, Finland

Abstract— **This paper presents a method for the rotor speed and position estimation of permanent magnet synchronous motors in a wide speed range including standstill. The proposed method is based on a modified voltage model at high speeds, and combines the modified voltage model with a high-frequency signal injection technique at low speeds. The fast dynamic response of the voltage model is thus augmented with the steady-state accuracy of the high-frequency signal injection technique. The stability and robustness of the combined observer are confirmed by simulations and experiments.**

I. Introduction

Vector control of a permanent magnet synchronous motor (PMSM) requires information of the rotor position. In sensorless control, the rotor speed and position are estimated without mechanical sensors either by a fundamental-excitation method or a signal injection method.

Fundamental-excitation methods are based on the dynamic model of the motor. The estimation algorithm can be a voltage model or a more complicated observer [1]–[4]. These methods are sensitive to the estimation of machine parameters. Since the back-emf is proportional to the rotor speed, problems are encountered at low speeds due to the limited accuracy of measurements and parameter estimates and due to the presence of inverter nonlinearities.

Signal injection methods are based on detecting the anisotropy caused by the saliency of the rotor or by magnetic saturation. A high-frequency (HF) test signal is superimposed on the stator voltage, and information of the rotor position is obtained from the current response [5]–[7]. If persistent HF excitation is used, the voltage carrier signal either revolves at high angular frequency [6]–[9] or alternates in the estimated rotor reference frame [10]–[14]. The rotor position can be estimated by a synchronous tracking scheme [6], [8], [10]–[13], which means that an error signal is driven to zero by the observer, or the rotor angle (or angle error) can be evaluated directly from the current response [7], [9], [14].

Fundamental-excitation methods have good dynamic properties, but they do not allow sustained operation at low speeds. On the other hand, signal injection methods are well suited to operation at low speeds, including standstill, but tend to have limited dynamic performance. Therefore, a combination of a fundamental-excitation method and an HF signal injection method might be a good solution when a wide speed range, including low-speed operation, is required. An approach for combining the methods was already discussed in [15]. A hybrid scheme combining a fundamental-wave flux observer with an HF signal injection method is proposed for the rotor flux estimation of induction motors in [16]. For PMSM drives, a fundamental-excitation method is used at higher speeds and a signal injection technique (or a combined method) at low speeds in [17]–[19].

This paper proposes a combined method, in which a modified voltage model is used throughout the whole speed range, and the estimation is augmented at low speeds with an HF signal injection technique. A voltage carrier signal alternating in the estimated rotor reference frame is used, and an error signal is obtained from the current response by a straightforward demodulation scheme. The error signal is driven to zero by a phase-locked loop (PLL) that also includes the output of the modified voltage model. The combination of two methods results in a simple observer having good steady-state accuracy and excellent dynamic properties over a wide speed range.

II. PMSM Model

The PMSM model is presented in the d-q reference frame fixed to the rotor. The d axis is oriented along the permanent magnet flux, whose angle in the stator reference frame is θ_m in electrical radians. The stator voltage components are

$$u_d = R_s i_d + \frac{d\psi_d}{dt} - \omega_m \psi_q \tag{1a}$$

$$u_q = R_s i_q + \frac{d\psi_q}{dt} + \omega_m \psi_d \tag{1b}$$

where i_d and i_q are the stator current components, R_s is the stator resistance, and $\omega_m = d\theta_m/dt$ the electrical angular speed of the rotor. The stator flux components are

$$\psi_d = L_d i_d + \psi_{pm} \tag{2a}$$

$$\psi_q = L_q i_q \tag{2b}$$

where L_d and L_q are the d- and q-axis inductances, respectively, and ψ_{pm} is the permanent magnet flux. The electromagnetic torque is given by

$$T_e = \frac{3}{2} p \left[\psi_{pm} i_q + (L_d - L_q) i_d i_q \right] \tag{3}$$

where p is the number of pole pairs.

 0-7803-8486-5/04/$20.00 © 2004 IEEE

III. Observer Structure

A. Modified Voltage Model

The pure voltage model suffers from drift problems due to the open-loop integration. The integration can be replaced by low-pass filtering and error compensation [20], [21].

The modified voltage model in the estimated rotor reference frame is formed from (1) and (2) as

$$\frac{d\hat{\psi}_{pm}}{dt} = \hat{e}_d + \alpha_v(\psi_{pm0} - \hat{\psi}_{pm}) \tag{4a}$$

$$\hat{\omega}_m = \frac{\hat{e}_q}{\hat{\psi}_{pm}} \tag{4b}$$

where the estimates of the back-emf components are

$$\hat{e}_d = u_d - \hat{R}_s i_d - \hat{L}_d \frac{di_d}{dt} + \hat{\omega}_m \hat{L}_q i_q \tag{5a}$$

$$\hat{e}_q = u_q - \hat{R}_s i_q - \hat{L}_q \frac{di_q}{dt} - \hat{\omega}_m \hat{L}_d i_d \tag{5b}$$

Estimates are marked by the symbol $\hat{}$, ψ_{pm0} is the presumed value of the permanent magnet flux, which can be obtained from an identification run, and α_v is a nonnegative gain. Furthermore, the estimate of the rotor position is obtained by integrating $\hat{\omega}_m$. The pure voltage model is obtained by choosing $\alpha_v = 0$. For $\alpha_v > 0$, the open-loop integrator is replaced with a low-pass filter having the bandwidth of α_v, and the error so introduced is compensated using ψ_{pm0}.

B. High-Frequency Signal Injection

An alternating voltage is used for HF signal injection [10]–[12]. A carrier excitation signal fluctuating at angular frequency ω_c and having amplitude $\hat{u}_c$, i.e.,

$$u_c = \hat{u}_c \cos(\omega_c t) \tag{6}$$

is superimposed on the d component of the stator voltage in the estimated rotor reference frame. An alternating HF current response is detected in the q direction of the estimated rotor reference frame, amplitude modulated by the rotor position estimation error. The principle of the demodulation scheme is shown in Fig. 1. The q component of the measured current is band-pass filtered (BPF), giving the current signal i_{qc} varying at the signal injection frequency. The current signal is then demodulated and low-pass filtered (LPF) to extract an error signal

$$\varepsilon = \mathrm{LPF}\{i_{qc} \sin(\omega_c t)\} \tag{7}$$

Ideally, this error signal is [10]

$$\varepsilon = \underbrace{\frac{\hat{u}_c}{\omega_c} \frac{L_q - L_d}{4L_q L_d}}_{K_\varepsilon} \sin(2\tilde{\theta}_m) \tag{8}$$

where K_ε is the signal injection gain and $\tilde{\theta}_m = \theta_m - \hat{\theta}_m$ is the estimation error of the rotor position.

The demodulation scheme is implemented as follows. Instead of using a band-pass filter, the filtering of i_q is achieved by

$$i_{qc} = i_q - \frac{1}{T_c} \int_{t-T_c}^{t} i_q dt \tag{9}$$

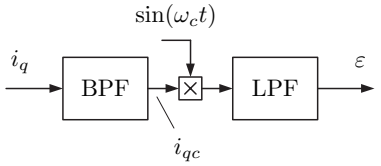

Fig. 1. Principle of the error signal demodulator.

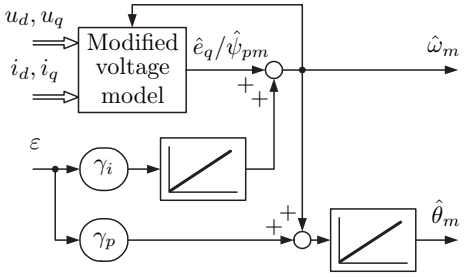

Fig. 2. Block diagram of the combined observer.

where $T_c = 2\pi/\omega_c$, i.e. by zero averaging over one period of the injection signal. The algorithm (9) can be interpreted as a high-pass filter, and its computational cost is lower than that of relevant band-pass filters. The low-pass filtering of the signal $i_{qc} \sin(\omega_c t)$ is implemented using two filters: a moving-average filter and a first-order low-pass filter. The moving-average filter removes the angular frequency ω_c and its multiples effectively and causes only a short time delay, while the first-order low-pass filter reduces stochastic noise more effectively than the moving-average filter. Due to the short delay of the moving-average filter, only the dynamics of the first-order low-pass filter are considered in the following. After filtering, the amplitude of ε is limited to avoid errors during transients.

C. Combined Observer

The combination of the modified voltage model and the HF signal injection method is illustrated in Fig. 2. The rotor speed and position estimates are obtained by

$$\hat{\omega}_m = \frac{\hat{e}_q}{\hat{\psi}_{pm}} + \gamma_i \int \varepsilon \, dt \tag{10a}$$

$$\hat{\theta}_m = \int (\hat{\omega}_m + \gamma_p \varepsilon) dt \tag{10b}$$

where γ_p and γ_i are positive gains, $\hat{\psi}_{pm}$ is estimated using (4a), and $\hat{e}_d$ and $\hat{e}_q$ (5) are evaluated using $\hat{\omega}_m$ from (10a). The HF signal injection and a PLL [15], [11] are used to augment the speed estimate obtained by the modified voltage model. The PI mechanism in (10) drives the error signal ε to zero in steady state. At low speeds, the combined observer relies both on the signal injection method and the voltage model: the signal injection method dominates in steady state whereas the voltage model commands at transients.

The PI mechanism used in a PLL can be tuned analytically [11]. The transfer function $\hat{\theta}_m(s)/\theta_m(s)$, corresponding to the linearized closed-loop system shown in Fig. 3, can be

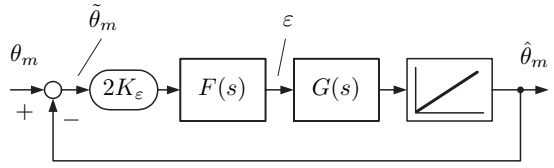

Fig. 3. Block diagram of the closed-loop system.

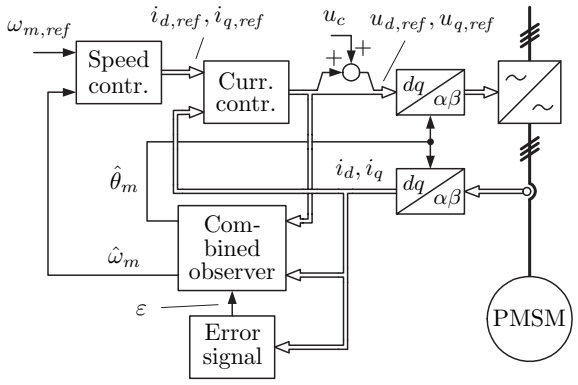

Fig. 4. Block diagram of the control system. Blocks "Error signal" and "Combined observer" are shown in Figs. 1 and 2, respectively. Block "Speed contr." includes both the speed controller and the minimization of the current amplitude.

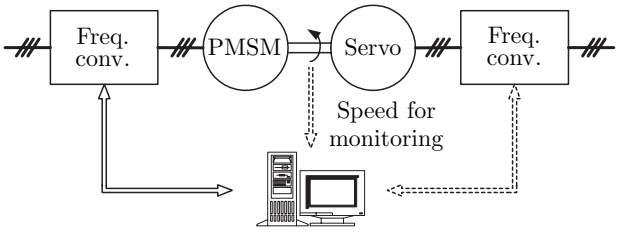

Fig. 5. Experimental setup. Mechanical load is provided by a servo drive.

TABLE I
MOTOR PARAMETERS

Nominal power	2.2 kW
Nominal/base voltage	370 V
Nominal/base current	4.3 A
Nominal/base frequency	75 Hz
Nominal speed	1 500 r/min
Nominal torque T_N	14.0 Nm
Number of pole pairs p	3
Stator resistance R_s	3.59 Ω
Direct axis inductance L_d	0.036 H
Quadrature axis inductance L_q	0.051 H
Permanent magnet flux ψ_{pm}	0.545 Vs
Total moment of inertia	0.015 kgm^2

used for determining the gains γ_p and γ_i. From (8), a linear approximation

$$\varepsilon \approx 2K_\varepsilon \tilde{\theta}_m \tag{11}$$

is used when determining the closed-loop transfer function. The influence of the voltage model is omitted, but the low-pass filter used in (7) is taken into account. The transfer function of the first-order low-pass filter having the bandwidth α_{lp} is

$$F(s) = \frac{\alpha_{lp}}{s + \alpha_{lp}} \tag{12}$$

and the transfer function of the PI mechanism is

$$G(s) = \gamma_p + \frac{\gamma_i}{s} \tag{13}$$

For the closed-loop system in Fig. 3, the transfer function is

$$\frac{\hat{\theta}_m(s)}{\theta_m(s)} = \frac{2K_\varepsilon \alpha_{lp}\gamma_p s + 2K_\varepsilon \alpha_{lp}\gamma_i}{s^3 + \alpha_{lp}s^2 + 2K_\varepsilon \alpha_{lp}\gamma_p s + 2K_\varepsilon \alpha_{lp}\gamma_i} \tag{14}$$

Placing all three poles of (14) to the point $-\alpha$ on the real axis yields the selection rule

$$\alpha_{lp} = 3\alpha \tag{15}$$

for the low-pass filter bandwidth and the selection rules

$$\gamma_p = \frac{\alpha}{2K_\varepsilon}, \quad \gamma_i = \frac{\alpha^2}{6K_\varepsilon} \tag{16}$$

for the gains of the PI mechanism. The proposed design method allows gain selection using only one design parameter α corresponding to the approximate bandwidth of the closed-loop system (14).

In order to obtain a smooth transition between the low-speed and high-speed regions, the injection voltage amplitude $\hat{u}_c$ and the bandwidth α are decreased linearly with increasing speed, and the signal injection is disabled above transition speed ω_Δ, i.e.,

$$\hat{u}_c = \begin{cases} \frac{\omega_\Delta - |\hat{\omega}_m|}{\omega_\Delta}\hat{u}_{c0}, & \text{if } |\hat{\omega}_m| \le \omega_\Delta \\ 0, & \text{if } |\hat{\omega}_m| > \omega_\Delta \end{cases} \tag{17a}$$

$$\alpha = \begin{cases} \frac{\omega_\Delta - |\hat{\omega}_m|}{\omega_\Delta}\alpha_0, & \text{if } |\hat{\omega}_m| \le \omega_\Delta \\ 0, & \text{if } |\hat{\omega}_m| > \omega_\Delta \end{cases} \tag{17b}$$

where $\hat{u}_{c0}$ and α_0 are the values corresponding to zero-speed operation. The parameters α_{lp} and γ_i are varied according to (15), (16), and (8). The parameter γ_p remains constant according to (16) and (8).

IV. CONTROL SYSTEM

The block diagram of the control system comprising cascaded speed and current control loops is shown in Fig. 4. The current control is implemented as PI-type control in the estimated rotor reference frame, where the cross-coupling terms and the back-emf are decoupled [22]. The current is predicted one sampling period ahead [23], [24]. The predicted current is used only in the proportional part of the PI controller to avoid steady-state error in the current response caused by parameter errors.

PI-type speed control with active damping is used. The current references $i_{d,ref}$ and $i_{q,ref}$ are calculated according to maximum torque per current control [25]. For position control, a P-type controller is added as the outermost control loop in the control system. The dc-link voltage of the converter is measured, and a simple current feedforward dead-time compensation is applied [26].

TABLE II
CONTROL SYSTEM PARAMETERS

Signal-injection angular frequency ω_c	2π1000 rad/s
Bandwidth α_0	2π20 rad/s
Voltage model gain α_v	2π15 rad/s
Current controller bandwidth	2π400 rad/s
Speed controller bandwidth	2π5 rad/s
Position controller bandwidth	2π1.33 rad/s

V. RESULTS

The proposed observer was investigated by means of simulations and laboratory experiments. The experimental setup is illustrated in Fig. 5. A 2.2-kW interior PMSM is fed by a frequency converter controlled by a dSPACE DS1103 PPC/DSP board. The motor parameters are given in Table I and the parameters of the control system in Table II. The dc-link voltage is 540 V. The sampling is synchronized to the modulation, and both the switching frequency and the sampling frequency are 5 kHz. The signal injection frequency is 1 kHz, and the transition speed $\omega_\Delta = 0.13$ p.u. The electromagnetic torque is limited to 22 Nm, i.e. $T_{max}/T_N = 1.57$. An incremental encoder is used to monitor the actual rotor speed and position, which is further used to calculate the rotor position estimation error.

The MATLAB/Simulink environment was used for the simulations. The parameters of the motor model used in the simulations correspond to the parameters of the motor used in the experiments. To incorporate the influence of parameter errors, the value of the stator resistance estimate was 20 % smaller than the stator resistance of the motor model. Moreover, white noise having an rms value of 10 mA was added to the measured phase currents of the motor, and the current signals were quantized in steps of 10 mA.

Fig. 6 shows simulation and experimental results at no load when the speed reference was changed stepwise from zero to 0.2 p.u. at t = 1 s, then reversed to -0.2 p.u. at t = 2 s, and finally set to zero at t = 3 s. The amplitude $\hat{u}_{c0}$ of the signal injection voltage was 20 V. The estimated rotor speed follows the actual speed smoothly. However, the rotor position estimate is noisy, especially in the experimental results, since the amplitude of the signal injection voltage is rather small in this experiment (3.7 % of the dc-link voltage).

Fig. 7 shows results corresponding to Fig. 6 when the amplitude $\hat{u}_{c0}$ of the signal injection voltage was increased to 50 V. The rotor position estimation error is less noisy, indicating a higher signal-to-noise ratio. At zero speed, the measured rms value of the HF current is 250 mA, i.e. 0.06 p.u. In the following examples, the voltage amplitude $\hat{u}_{c0} = 50$ V is used (although the value $\hat{u}_{c0} = 20$ V also results in stable operation). In Figs. 6(b) and 7(b), a periodic variation can be seen in the rotor position estimation error between t = 1 s and t = 3 s. The variation is caused by a small eccentricity of the incremental encoder assembly.

Fig. 8 depicts simulation and experimental results when the speed reference was set to zero. The load torque was first changed stepwise from zero to the nominal value at t = 1 s,

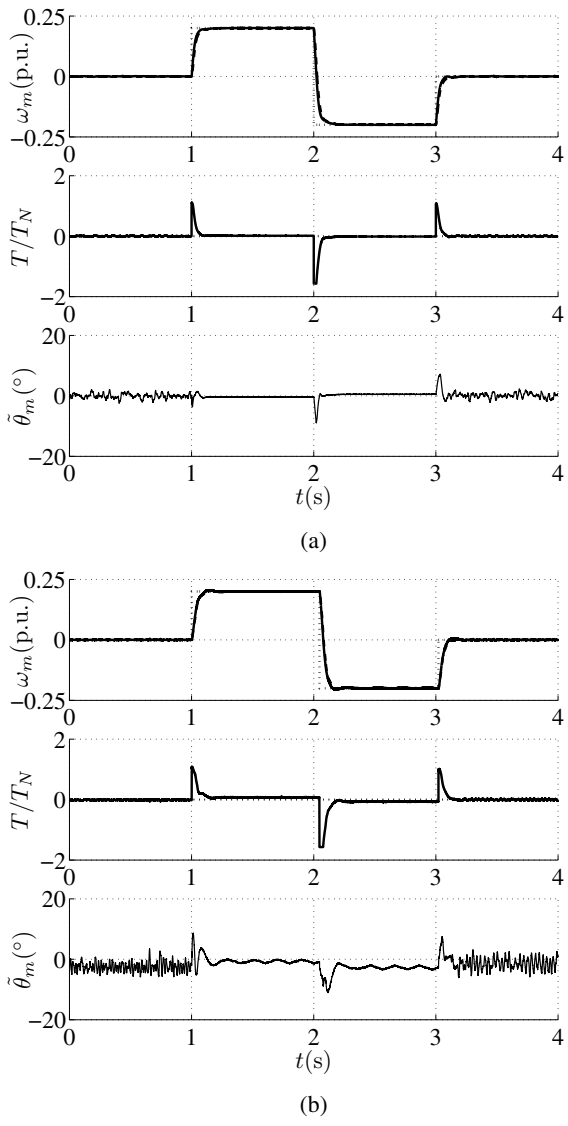

Fig. 6. Speed reference steps at zero load torque for $\hat{u}_{c0} = 20$ V: (a) simulation results; (b) experimental results. First subplot shows electrical angular speed (solid), its estimate (dashed), and its reference (dotted). Second subplot shows estimated electromagnetic torque (solid) and load torque reference (dotted). Last subplot shows estimation error of rotor position in electrical degrees.

then reversed at t = 2 s, and removed at t = 3 s. The error of the rotor position estimate is small even during transients, indicating good dynamic performance. Furthermore, it can be seen that the experimental results correspond well to the simulation results.

Simulation and experimental results at the nominal load torque are shown in Fig. 9. The speed reference was first changed stepwise from zero to 0.66 p.u. at t = 1 s, then reversed to -0.66 p.u. at t = 2 s, and finally set to zero at t = 3 s. The estimated rotor speed follows the actual speed smoothly even during the transitions between the voltage model and the combination of the voltage model and HF signal injection.

Fig. 10 shows simulation and experimental results for the position control at nominal load torque. The position refer-

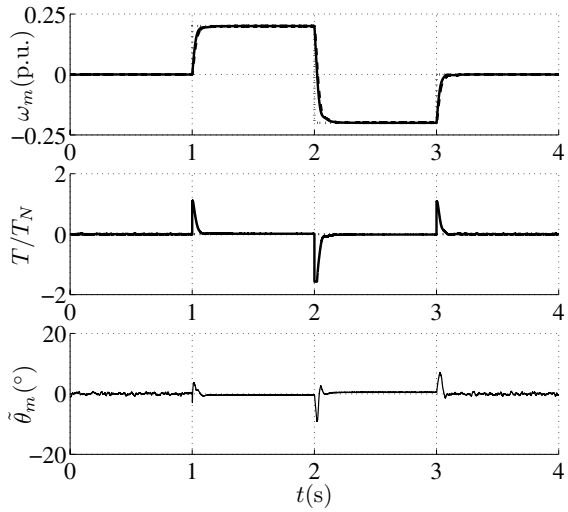

(a)

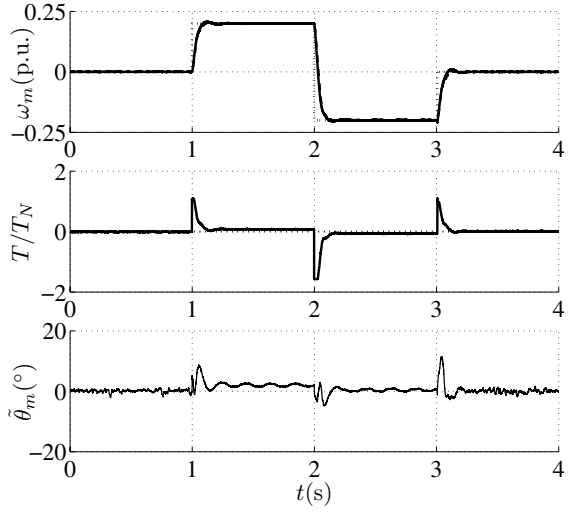

(b)

Fig. 7. Speed reference steps at zero load torque for $\hat{u}_{c0} = 50$ V: (a) simulation results; (b) experimental results. Explanations of the curves are as in Fig. 6.

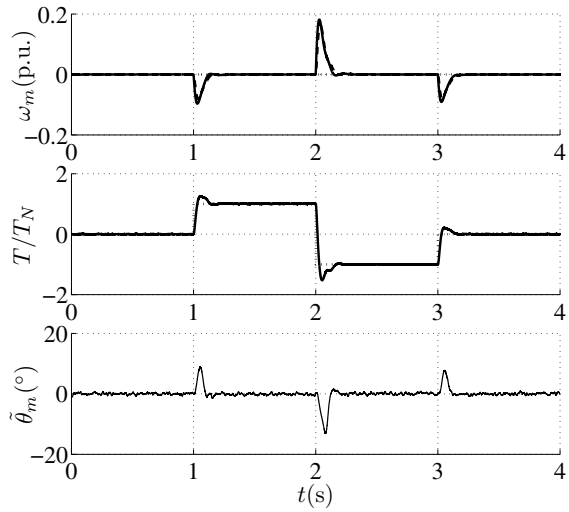

(a)

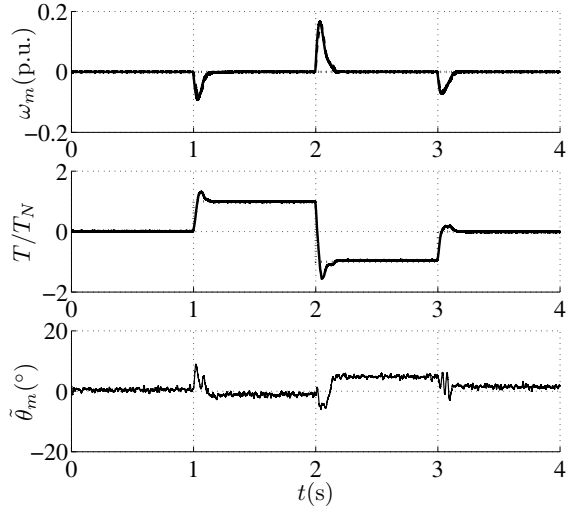

(b)

Fig. 8. Nominal load torque steps at zero speed reference: (a) simulation results; (b) experimental results. Explanations of the curves are as in Fig. 6.

ence was changed stepwise from zero to one revolution (6π electrical radians) at t = 1 s, then two revolutions backwards at t = 2 s, and finally set to zero at t = 3 s. The position estimate follows the actual value smoothly, and the position settles quickly to its reference value.

VI. Conclusions

The rotor speed and position of a permanent magnet synchronous motor can be estimated in a wide speed range, including zero speed, by means of a modified voltage model that is augmented with a high-frequency signal injection technique at low speeds. The fast dynamic response of the voltage model is combined with the steady-state accuracy of the high-frequency signal-injection method. The signal injection scheme is based on a voltage carrier signal alternating in the estimated rotor reference frame and simple demodulation of the current response. Guidelines for the gain selection of the tracking observer are obtained analytically. According to the simulations and experiments presented in the paper, the system based on the combined observer is stable and robust, and can cope with stepwise changes in the speed or position reference and with nominal load torque steps.

Acknowledgment

The authors gratefully acknowledge the financial support given by ABB Oy and the Finnish Cultural Foundation.

References

[1] R. Wu and G. R. Slemon, "A permanent magnet motor drive without a shaft sensor," *IEEE Trans. Ind. Applicat.*, vol. 27, no. 5, pp. 1005–1011, Sept./Oct. 1991.

[2] R. B. Sepe and J. H. Lang, "Real-time observer-based (adaptive) control of a permanent-magnet synchronous motor without mechanical sensors," *IEEE Trans. Ind. Applicat.*, vol. 28, no. 6, pp. 1345–1352, Nov./Dec 1992.

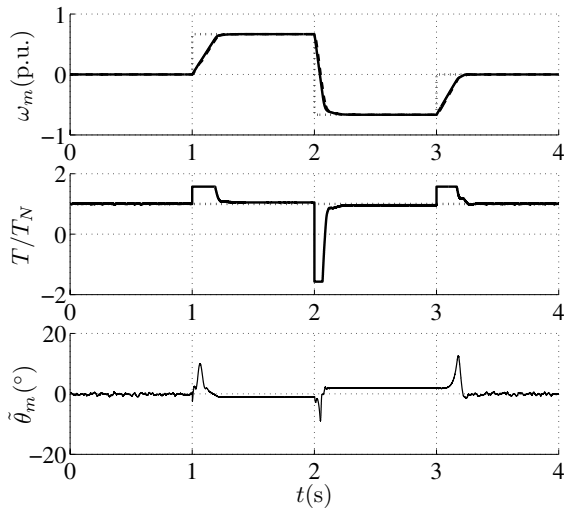

(a)

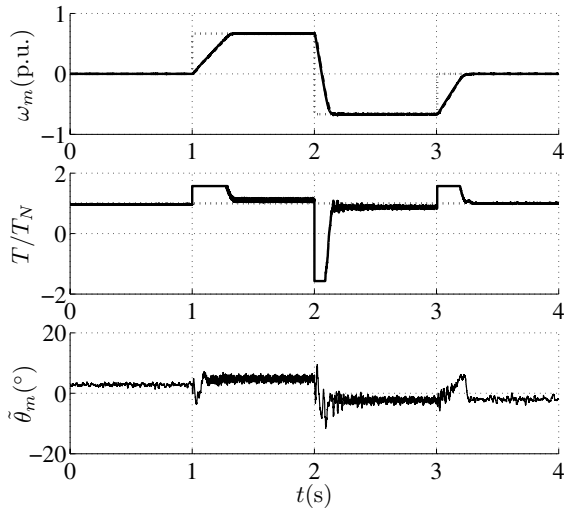

(b)

Fig. 9. Speed reference steps at nominal load torque: (a) simulation results; (b) experimental results. Explanations of the curves are as in Fig. 6.

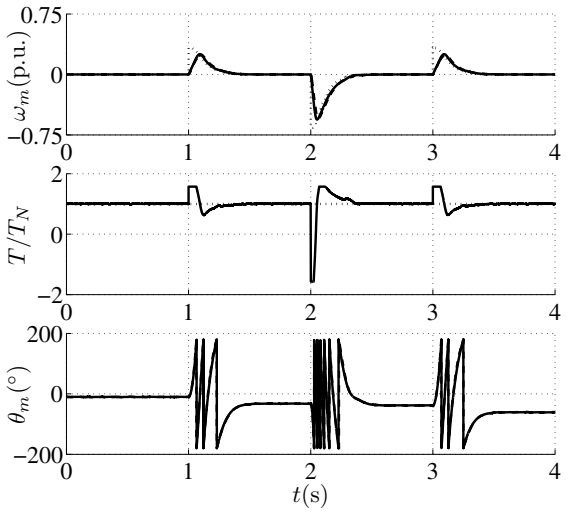

(a)

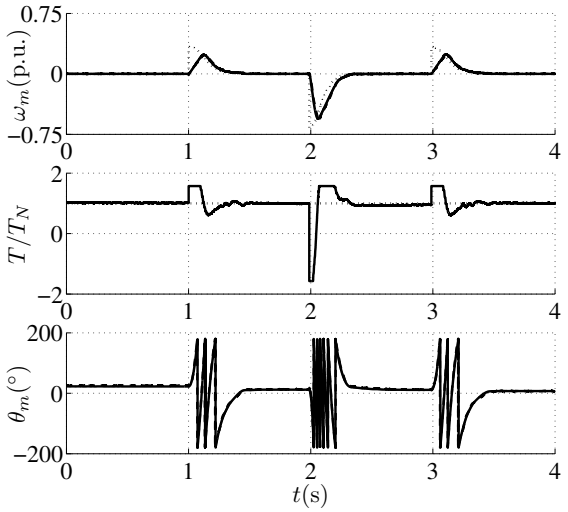

(b)

Fig. 10. Position reference steps at nominal load torque: (a) simulation results; (b) experimental results. First subplot shows electrical angular speed (solid), its estimate (dashed), and its reference (dotted). Second subplot shows estimated electromagnetic torque (solid) and load torque reference (dotted). Last subplot shows rotor position (solid) and its estimate (dashed) in electrical degrees.

[3] J. Solsona, M. I. Valla, and C. Muravchik, "A nonlinear reduced order observer for permanent magnet synchronous motors," *IEEE Trans. Ind. Electron.*, vol. 43, no. 4, pp. 492–497, Aug. 1996.

[4] S. Bolognani, R. Oboe, and M. Zigliotto, "Sensorless full-digital PMSM drive with EKF estimation of speed and rotor position," *IEEE Trans. Ind. Electron.*, vol. 46, no. 1, pp. 184–191, Feb. 1999.

[5] M. Schroedl, "Sensorless control of AC machines at low speed and standstill based on the INFORM method," in *Conf. Rec. IEEE-IAS Annu. Meeting*, vol. 1, San Diego, CA, Oct. 1996, pp. 270–277.

[6] P. L. Jansen and R. D. Lorenz, "Transducerless position and velocity estimation in induction and salient AC machines," *IEEE Trans. Ind. Applicat.*, vol. 31, no. 2, pp. 240–247, March/April 1995.

[7] A. Consoli, G. Scarcella, and A. Testa, "Industry application of zero-speed sensorless control techniques for PM synchronous motors," *IEEE Trans. Ind. Applicat.*, vol. 37, no. 2, pp. 513–521, March/April 2001.

[8] L. Wang and R. D. Lorenz, "Rotor position estimation for permanent magnet synchronous motor using saliency-tracking self-sensing method," in *Conf. Rec. IEEE-IAS Annu. Meeting*, vol. 1, Rome, Italy, Oct. 2000, pp. 445–450.

[9] C. Silva, G. M. Asher, M. Sumner, and K. J. Bradley, "Sensorless rotor position control in a surface mounted PM machine using HF rotating injection," *EPE Journal*, vol. 13, no. 3, pp. 12–18, Aug. 2003.

[10] M. Corley and R. D. Lorenz, "Rotor position and velocity estimation for a salient-pole permanent magnet synchronous machine at standstill and high speeds," *IEEE Trans. Ind. Applicat.*, vol. 43, no. 4, pp. 784–789, July/Aug. 1998.

[11] L. Harnefors and H.-P. Nee, "A general algorithm for speed and position estimation of AC motors," *IEEE Trans. Ind. Electron.*, vol. 47, no. 1, pp. 77–83, Feb. 2000.

[12] M. Linke, R. Kennel, and J. Holtz, "Sensorless position control of permanent magnet synchronous machines without limitation at zero speed," in *Proc. IEEE IECON'02*, vol. 1, Sevilla, Spain, Nov. 2002, pp. 674–679.

[13] J. H. Jang, S. K. Sul, J. I. Ha, K. Ide, and M. Sawamura, "Sensorless drive of SMPM motor by high frequency signal injection," in *Proc. IEEE APEC'02*, vol. 1, Dallas, TX, March 2002, pp. 279–285.

[14] F. Parasiliti, R. Petrella, and M. Tursini, "Sensorless speed control of salient rotor PM synchronous motor based on high frequency signal injection and kalman filter," in *Proc. IEEE ISIE'02*, vol. 2, L'Aquila, Italy, July 2002, pp. 623–628.

[15] P. L. Jansen, M. J. Corley, and R. D. Lorenz, "Flux, position, and velocity estimation in ac machines at zero and low speed via tracking of high frequency saliencies," in *Proc. EPE'95*, vol. 3, Sevilla, Spain, Sept. 1995, pp. 154–159.

[16] K. Ide, J.-I. Ha, M. Sawamura, H. Iura, and Y. Yamamoto, "A novel hybrid speed estimator of flux observer for induction motor drives," in *Proc. IEEE ISIE'02*, vol. 3, L'Aquila, Italy, July 2002, pp. 822–827.

[17] E. Robeischl, M. Schroedl, and M. Krammer, "Position-sensorless biaxial position control with industrial PM motor drives based on INFORM- and back EMF model," in *Proc. IEEE IECON'02*, vol. 1, Sevilla, Spain, Nov. 2002, pp. 668–673.

[18] C. Silva, G. M. Asher, and M. Sumner, "An hf signal-injection based observer for wide speed range sensorless PM motor drives including zero speed," in *Proc. EPE'03*, vol. 1, Toulouse, France, Sept. 2003, pp. 1–9.

[19] M. Tursini, R. Petrella, and F. Parasiliti, "Sensorless control of an IPM synchronous motor for city-scooter applications," in *Conf. Rec. IEEE-IAS Annu. Meeting*, vol. 3, Salt Lake City, UT, Oct. 2003, pp. 1472–1479.

[20] T. Ohtani, N. Takada, and K. Tanaka, "Vector control of induction motor without shaft encoder," *IEEE Trans. Ind. Applicat.*, vol. 28, no. 1, pp. 157–164, Jan./Feb. 1992.

[21] H. Rasmussen, P. Vadstrup, and H. Borsting, "Sensorless field oriented control of a pm motor including zero speed," in *Proc. IEEE IEMDC'03*, vol. 2, Madison, WI, June. 2003, pp. 1224–1228.

[22] F. Briz del Blanco, M. W. Degner, and R. D. Lorenz, "Dynamic analysis of current regulators for AC motors using complex vectors," *IEEE Trans. Ind. Applicat.*, vol. 35, no. 6, pp. 1424–1432, Nov./Dec. 1999.

[23] J. Böcker, J. Janning, and K. Anbuhl, "Realization of a high-dynamic discrete-time controller for PWM inverter-fed induction motor drives," in *Proc. EPE'93*, vol. 4, Brighton, UK, Sept. 1993, pp. 158–162.

[24] L. Springob and J. Holtz, "High-bandwidth current control for torque-ripple compensation in PM synchronous machines," *IEEE Trans. Ind. Electron.*, vol. 45, no. 5, pp. 713–721, Oct. 1998.

[25] T. Jahns, G. Kliman, and T. Neumann, "Interior permanent-magnet synchronous motors for adjustable-speed drives," *IEEE Trans. Ind. Applicat.*, vol. 22, no. 4, pp. 738–747, July/Aug. 1986.

[26] J. K. Pedersen, F. Blaabjerg, J. W. Jensen, and P. Thogersen, "An ideal PWM-VSI inverter with feedforward and feedback compensation," in *Proc. EPE'93*, vol. 5, Brighton, UK, Sept. 1993, pp. 501–507.